Progress In Electromagnetics Research C, Vol. 87, 51–62, 2018

Investigating the Performance of a Fully Laminated Flux-Focusing Magnetic Gearbox

Kang Li[1], Kiran Uppalapati[1], Jason Wright[1], Joshua Kadel[2], Jonathan Z. Bird[3, *], and Wesley Williams[2]

Abstract—This paper presents the design investigation and experimental testing of a flux-focusing magnetic gearbox with a fully laminated rotor structure. The unique feature of this flux-focusing magnetic gearbox design is that the three rotors are each made of a single lamination stack, and the central modulation structure is retained in place without the use of a resin filler such as epoxy. Ferromagnetic bridges are used to connect individual pole pieces together. It is shown that the use of the ferromagnetic bridges reduces the calculated torque density from 156 Nm/L to 139 Nm/L (a reduction of 11%). The experimentally measured torque density is, however, only 97 Nm/L. The reason for this discrepancy is associated with the demagnetization of the magnets.

1. INTRODUCTION

A magnetic gearbox (MG) utilizes magnetic field heterodyning to create speed amplification without physical contact. MGs have an inherent torque overload capability and they have the potential for quiet operation and high conversion efficiency [1–5]. The lack of physical contact between rotors enables the MG to be highly reliable and the MG does not require lubrication. This therefore reduces the gearboxes maintenance costs. An example of a coaxial flux-focusing MG is shown in Figure 1. In this typology the inner and outer rotors contains p_1 pole-pairs and p_3 pole-pairs respectively. It was first shown by Martin [1] that by inserting n_2 ferromagnetic slots between the rotors such that

$$n_2 = p_1 + p_3 \tag{1}$$

the rotors can create a non-zero average torque. The angular speed relationship between each rotor is then [1, 2]

$$n_2\omega_2 = p_1\omega_1 + p_3\omega_3 \tag{2}$$

where the subscripts denote rotor number. If the outer rotor is fixed ($\omega_3 = 0$) the speed ratio is

$$\omega_1 = G_{12}\omega_2 \tag{3}$$

where $G_{12} = n_2/p_1$. For the example shown in Figure 1 the gear ratio is $G_{12} = 4.25$. By making the magnet surface area larger than the ferromagnetic surface area facing the air-gap the flux focusing design, as shown in Figure 1, can increase the air-gap flux density [6], and therefore a higher torque density can be achieved than when using a surface mounted magnet rotor design.

The active region volumetric torque density of an MG is defined as

$$T_v = T_2 / (\pi r_{o3}^2 d) \tag{4}$$

where r_{o3} = outer radius of MG and d = axial stack length.

Received 25 June 2018, Accepted 31 August 2018, Scheduled 17 September 2018

* Corresponding author: Jonathan Bird (jonathan.bird@ieee.org).

[1] Department of Electrical and Computer Engineering, University of North Carolina at Charlotte, 9201 University City Boulevard, Charlotte, NC 29223, USA. [2] Department of Engineering Technology, University of North Carolina at Charlotte, 9201 University City Boulevard, Charlotte, NC 29223, USA. [3] Laboratory for Electromagnetic Energy Conversion and Control, Department of Electrical and Computer Engineering Portland State University, Portland, OR, USA.

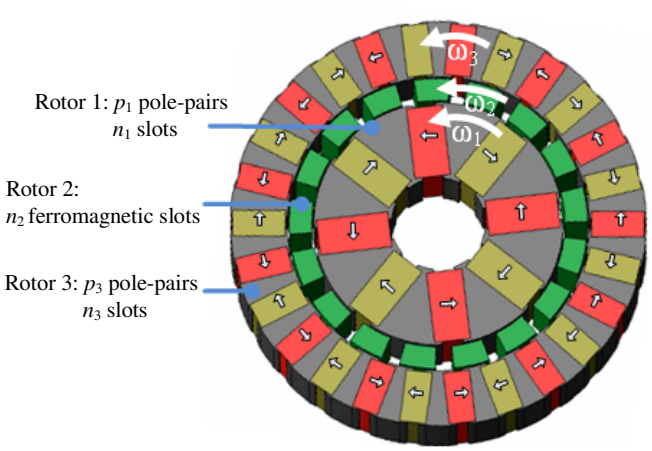

Figure 1. A 4.25 : 1 coaxial flux-focusing magnetic gearbox using flux focusing PMs. $p_1 = 4$ pole-pairs, $n_2 = 17$ steel poles and $p_3 = 13$ pole-pairs on the outer rotor [7].

Coaxial MGs have been experimentally shown to be capable of achieving active region torque densities above 200 Nm/L [8]. However, further improvements in torque density, efficiency and manufacturability are still needed in order to make the MG competitive with mechanical gearboxes. The central rotor, called the cage rotor in this paper, is particularly difficult to design as it is subjected to the highest torque and experiences large oscillatory radial and azimuthal forces [9, 10].

Atallah et al. constructed an MG in which the cage rotor was made of one laminated piece with outer radius bridges [2]. The laminations were supported in place by using epoxy and stainless steel rods within the spaces between the steel. Around the same time, Rasmussen et al. independently designed an MG [3] using a flux-focusing inner rotor and surface mounted outer magnets. The central steel segmented rotor was retained in place using nylon and stainless-steel rods. Rasmussen et al. and Gerber et al. used bridges on the inside diameter of the cage rotor with steel rods embedded in epoxy within the cage rotor spacing [11, 12]. In a later design Rasmussen used a composite bar to secure the cage rotor in place [13]. Frank and Toliyat constructed an MG using bridges on both the inner and outer cage rotor radii [14]. Gerber and Wang also used this approach [12]. Rasmussen et al. [11], Gouda [15], Kowol et al. [16] and the authors of this paper tried constructing an MG cage rotor using soft magnetic composite (SMC) magnetic material. The authors' SMC rotor is shown in Figure 2(a). The SMC material is incredibly brittle and therefore retaining it in place is difficult for an MG application. Uppalapati et al. constructed an MG using solid steel bar segments [7, 8]. Uppalapati et al. showed that due to high eddy current loss, solid steel bars can only be used when operating at a very low input speed. The authors along with Kowol [16] also recently constructed a cage rotor using laminations stacked along the azimuthal length, as shown in Figure 2(b) while this significantly reduces losses the laminations are mechanically difficult to retain in place. Kim et al. proposed using circular non-magnetic cage rotor support rods in [17], Kim simulations showed this could reduce torque ripple. However, an experimental prototype was not presented. Liu et al. used an interesting slotted laminated structure to maintain individual lamination stacks in place in a magnetically geared generator [18].

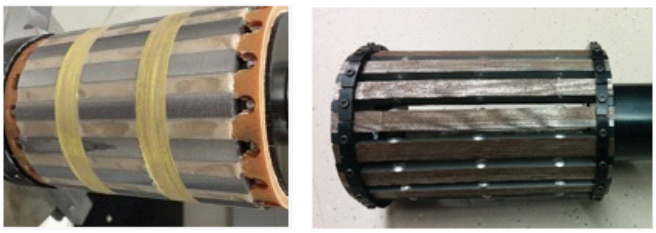

(a) (b)

Figure 2. (a) A soft magnetic composite rotor structure, a Kevlar band is used to hold the composite in place, (b) a laminated cage rotor with laminations stacked along the azimuthal direction.

Most cage rotor designs provide axial bearing support on both sides of the stack length. However, Jian et al. and Gerber et al. successfully tested an MG in which the cage rotor laminations were supported on only one axial side of the rotor [12, 19]. Due to the large radial forces such an approach could only be used when the axial length is relatively small.

Designs that require the cage rotor to be made with epoxy casting or are made from many individual ferromagnetic steel pieces will significantly increase construction costs, use many individual parts, and also create tolerance and alignment challenges. This paper looks at the different design trade-offs when modifying an MG with the emphasis on trying to design a low assembly cost MG structure whilst still retaining a relatively high torque density. This research builds on the work presented in [7] and [20] and investigates the performance of using a fully laminated coaxial MG without any epoxy casting. A similar cage rotor approach was recently studied by Nobuhara et al. [21]; however, this was for a surface mounted MG motor.

2. DESIGN ANALYSIS

The flux-focusing design shown in Figure 1 was calculated using finite element analysis (FEA) to be able to operate with a volumetric torque density of $T_v = 156\,\mathrm{Nm/L}$ when using the parameters given in Table 1. However, this design is not practical from an assembly perspective because the steel poles are made of individual ferromagnetic segments [7]. In order to develop a lower assembly cost design, a range of different design changes were considered, as shown in Table 2. A summary of the corresponding peak torque and the torque ripple calculated using 2-D FEA for each design is shown in Table 2. Design VI–Design XIII use the same amount of magnet volume.

Designs I, II and III look at different steel pole configurations that will retain the magnets in place without the need for the tooth tips as used by the design shown in Figure 1. The azimuthally directed flux-focusing magnetization direction is shown for Design I. All other designs shown in Figure 3 use the same magnetization directions as that shown for Design I. The blue circles shown in Figure 3 are the ferromagnetic rods that retain the lamination stack in place via axially placed end-plates. Designs I and III have higher torque than the original design however Design II has lower torque due to the leakage that is created through the inner rotor retaining bars. This leakage is illustrated in Figure 4.

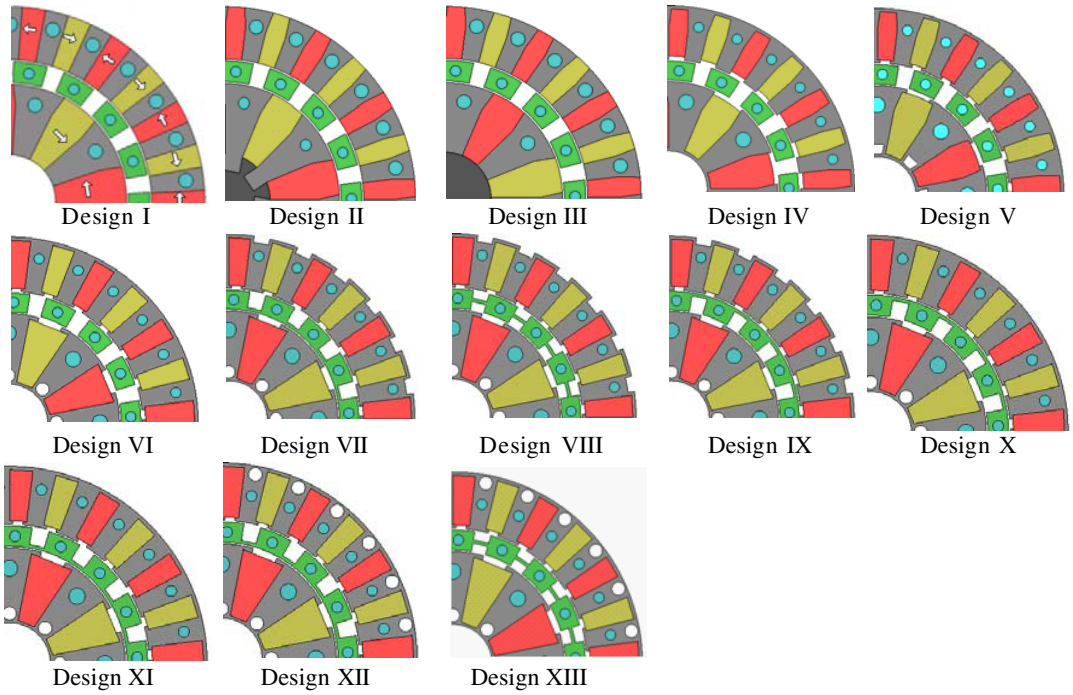

Figure 3. Design topologies that were studied.

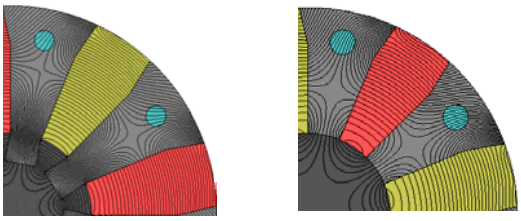

(a) (b)

Figure 4. Magnetic vector potential field lines for the inner rotor for (a) Design II and (b) Design III. The increased inner shaft field leakage in Design II is clearly evident.

Table 1. Geometric parameters and material properties.

Inner rotor	Pole pairs, p_1	4	-
	Inner radius, r_{i1}	12	mm
	Outer radius, r_{o1}	33	mm
	Steel pole span, θ_{s1}	$\pi/8$	rad.
	Airgap, g	0.5	mm
Cage rotor	Steel poles, n_2	17	-
	Inner radius, r_{i1}	33.5	mm
	Outer radius, r_{o1}	39.5	mm
	Steel pole span, θ_{s2}	$7\pi/90$	rad.
Outer rotor (stationary)	Pole pairs, p_3	13	-
	Inner radius, r_{i3}	40	mm
	Outer radius, r_{o3}	56	mm
	Steel pole span, θ_{s3}	$\pi/26$	rad.
	Airgap, g	0.5	mm
Material	Magnet, NdFeB, N40H, B_r	1.28	T
	Laminations, M19 C5 G26	-	-
Active region stack length, d		75	mm

Designs IV, V and VI look at the effect of adding steel bridges on the inner radius of the inner rotor and the outer radius of the outer rotor. Comparing Designs III and IV one can note that the bridges reduce the torque by 5%. In Designs V and VI flux leakage barriers (holes) have been inserted around the base of the inner rotor. In addition, magnet retaining lips have been added. The flux leakage barriers increase torque slightly while the magnet retaining lips reduce the torque. The overall change is therefore minimal when compared to Design IV.

Designs VII, VIII and IX look at the effect of adding steel bridges on the cage rotor. In addition, rectangular leakage barriers were added on the outer radius of the outer rotor. It can be seen from Table 2 that adding the bridges on the inner radius or center reduces the torque by $\sim 7\%$ compared to Design VI while adding the bridge on the outer radius reduces peak torque by 14% compared to Design VI. Locating the cage rotor bridge near the inner radius or center of the cage rotor results in a relatively large torque ripple being created whereas putting the bridge at the outer radius (Design IX) results in a low torque ripple but this also significantly reduces the peak torque. Based on these three designs it appears that there is a trade-off between achieving a low torque ripple or high peak torque. If one now considers Designs X and XI in which the rectangular outer rotor leakage slots have been removed one can see that removing this outer rectangular slot does not change the torque ripple significantly (compared to Designs VII and IX). However, if the outer rotor rectangular leakage slot in Design VII is replaced with a circular hole as in Design XII, it can be noted that the torque ripple drops significantly, and torque increases slightly. Therefore, in this design the circular hole helps to reduce torque ripple.

Table 2. Torque performance comparison.

Design Change	Design #	Torque [Nm]	Torque density [Nm/L]	Torque ripple [Nm]		Bridge type*
				Outer rotor	Inner rotor	
-	Original	115	156.6	0.2	0.4	n
No retaining magnet tips	I	119.6	161.9	0.42	1.5	n
	II	111	150.2	-	-	n
	III	119	161.0	-	-	n
· Outer rotor lamination bridges · Inner rotor flux barrier holes	IV	113	152.9	-	-	n
	V	111.8	151.3	-	-	n
	VI	112.8	152.7	0.2	0.1	n
· Cage rotor bridges · Rectangular outer rotor leakage barriers	VII	105.2	142.1	2.2	0.4	i
	VIII	103.5	140.0	0.75	0.25	m
	IX	96.9	131.0	0.2	0.14	o
· No rectangular outer rotor leakage barriers	X	105.2	142.4	2.2	0.6	i
	XI	95.8	129.7	0.175	0.14	o
Outer rotor flux barrier holes	XII	105.8	143.2	0.9	0.4	i
	XIII	103	139.4	0.3	0.15	m
Added retaining sleeve slots	XIV	103.1	139.5	0.35	0.2	m

*Key: n = no bridge; o = outer radius bridge; i = inner radius bridge; m = middle bridge

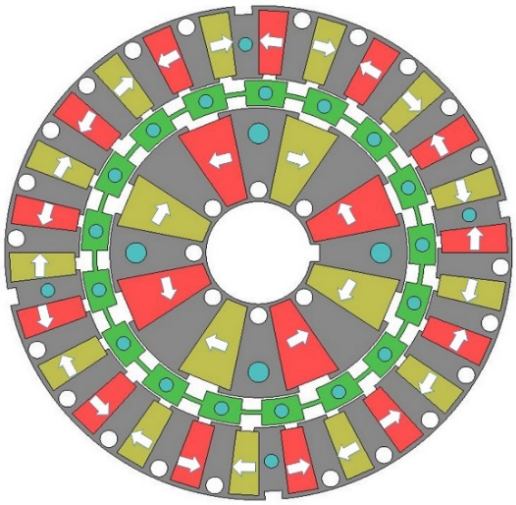

Figure 5. The final laminated design (Design XIV) with magnet orientation shown.

Design XIII shifts the cage rotor bridge to the center, and one can see that the torque ripple goes down considerably, but the peak torque is only reduced by 2.8 Nm; therefore, Design XIII was selected. The final design (Design XIV) is shown in Figure 5. Design XIV differs slightly from Design XIII in that additional outer and inner slots were added for mechanical outer sleeve retention purposes. Table 2 shows that this minor design change makes marginal difference.

3. FIELD AND TORQUE ANALYSIS

The radial and azimuthal magnetic flux density field values within the Design XIV MG are shown in Figure 6. Saturation around the inner and outer rotor bridges and the flux barrier hole is evident. Figure 6(b) shows that the flux barrier holes prevent a large amount of radial leakage flux from passing

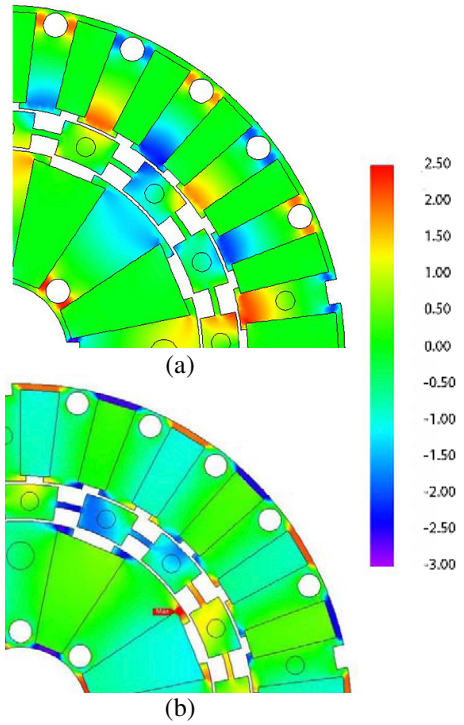

Figure 6. (a) Radial flux density, B_r, and (b) azimuthal flux density, B_θ surface plot for Design XIV.

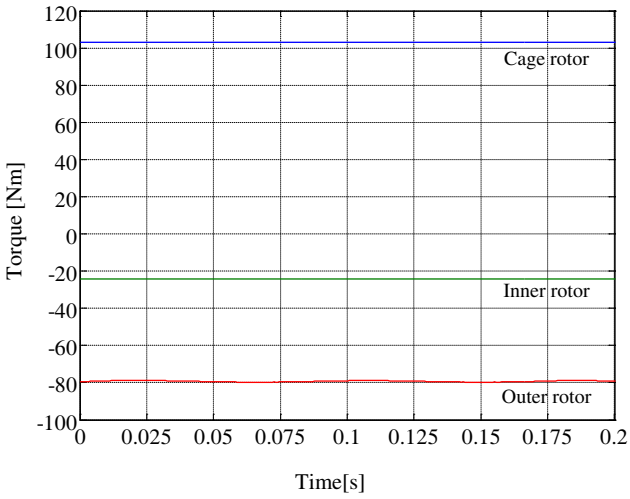

Figure 7. Calculated torque as a function of time at peak torque condition.

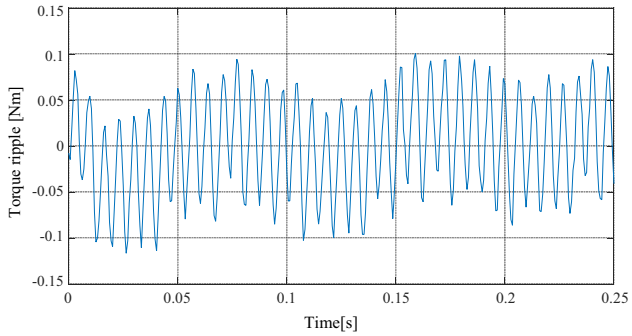

Figure 8. Calculated High-speed (inner rotor) torque ripple.

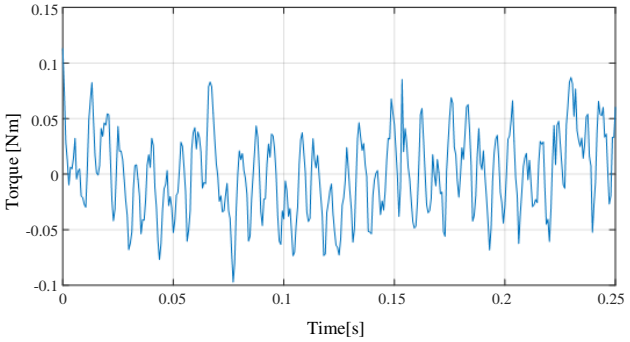

Figure 9. Calculated Low-speed rotor (cage rotor) torque ripple.

through the bridges, and this, therefore, increases the MG torque density. The 2-D FEA calculated torque and torque ripple for Design XIV is plotted in Figure 7–Figure 9 for the peak torque condition. A very low torque ripple was calculated.

4. EXPERIMENTAL PROTOTYPE

The experimental prototype drawing for the MG (Design XIV) is shown in Figure 10. The outer and inner rotors are held in place using both a keyway and end-plates. The central cage rotor (rotor 2) is held together using end-plates and ferromagnetic steel rods. The rods run through the center of the cage rotor bars. The rotor laminations are shown in Figure 11 and the inner rotor (without magnets) as well as the cage rotor with endplates is shown in Figure 12.

The MG mounted on the test-stand is shown in Figure 13. Torque transducers and encoders on the high and low speed rotor sides were used to measure both torque and speed. The measured torque and torque ripple at peak torque condition are shown in Figure 14 and Figure 15. Unfortunately, the measured torque was significantly lower than expected. The peak torque was measured to be only $T_2 = 71.7\,\text{Nm}$ (97 Nm/L) which is 30% lower than the 2-D calculated value. The torque ripple is

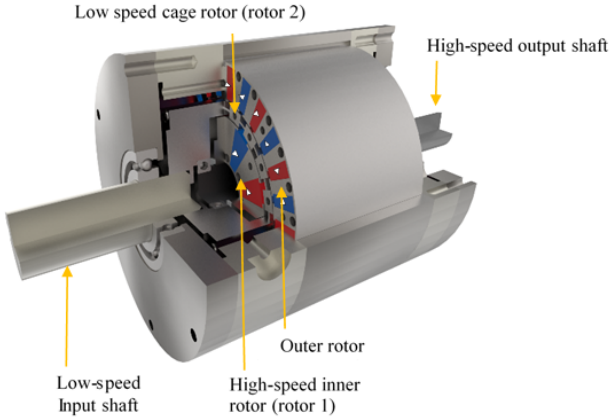

Figure 10. Mechanical assembly.

Figure 11. Rotor laminations (outer, cage, and inner).

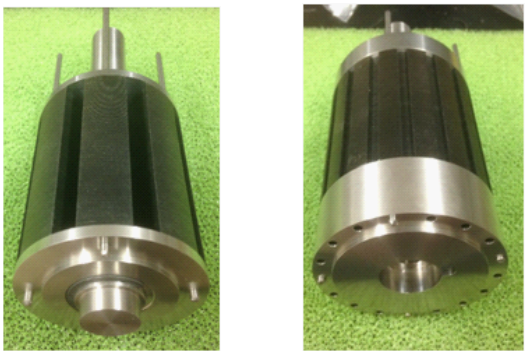

Figure 12. (a) Inner rotor (without magnets) and (b) cage rotor during assembly.

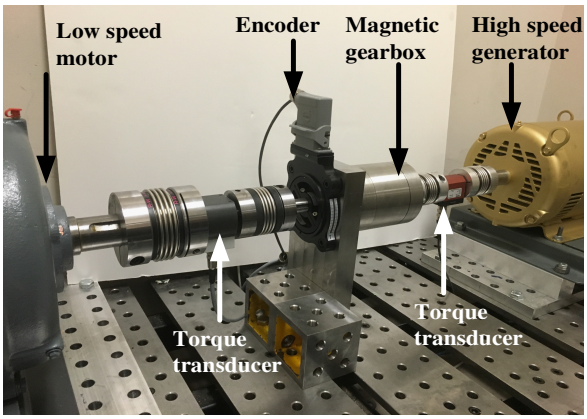

Figure 13. Mechanical testing setup.

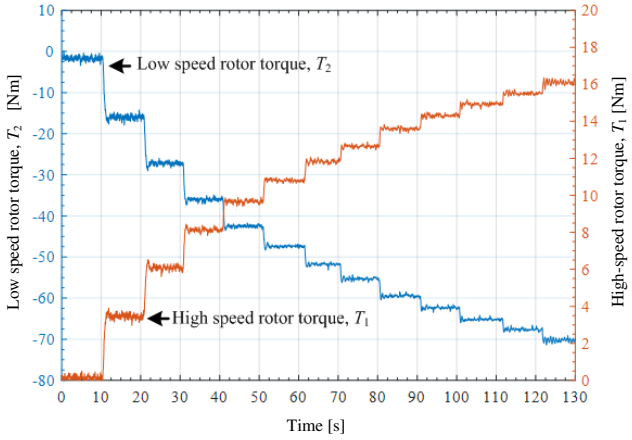

Figure 14. Measured torque vs. time on low-speed (rotor 2) and high-speed rotor (rotor 1) when $\omega_1 = 123$ RPM.

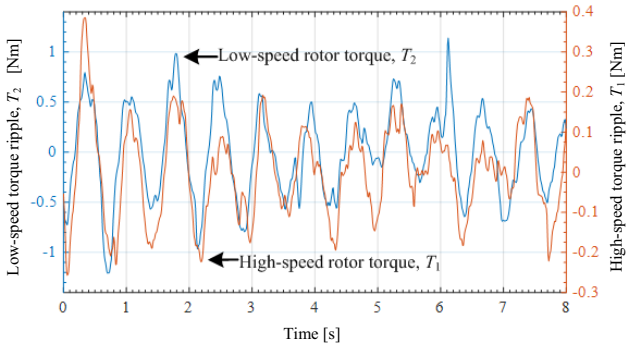

Figure 15. Measured torque ripple vs. time on low speed (rotor 2) and high-speed rotor (rotor 1) at peak torque condition.

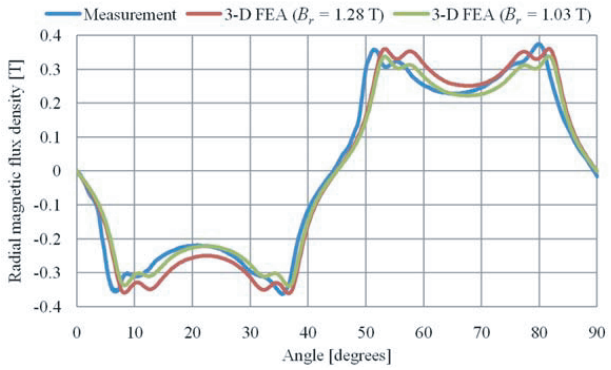

(a)

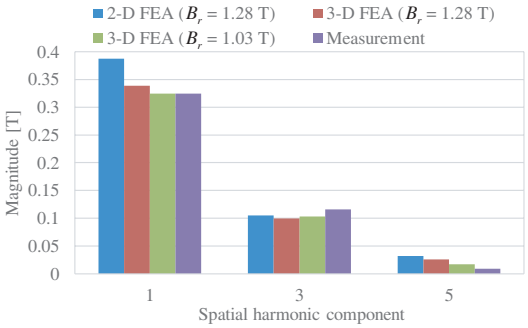

(b)

Figure 16. Inner rotor field comparison when the inner rotor is surrounded by air (measured at 1 mm above the rotor surface) for $B_r = 1.28$ T and $B_r = 1.03$ T, (a) field plot and (b) harmonic analysis.

also significantly higher than calculated which is believed to be due to the mechanical misalignments introduced within the rotor parts after repeated disassembly and reassembly. Earlier testing indicated a lower torque ripple; however, only the final assembled MG torque ripple is reported here. The reason for the lower peak torque is discussed in the next section.

5. PEAK TORQUE DISCREPANCY ANALYSIS

In order to understand why the MG had significantly lower measured torque than expected, it was disassembled (multiple times), and the magnetic flux density of the inner rotor, when being surrounded by air, was measured. The field measurements are shown in Figure 16(a) while Figure 16(b) compares the calculated 1st, 3rd and 5th order spatial field harmonic values with the measured value. It shows that the 3-D FEA model more closely predicts the measured field magnitude. However, the fundamental field calculated using the 3-D model is still 4.3% higher. The magnet's residual flux density had to be lowered to $B_r = 1.03$ T in order to obtain a match with the fundamental field component when using the 3-D model. By measuring the individual magnets field, as shown in Figure 17 one can clearly see that the magnet's field is close to the expected value when using $B_r = 1.03$ T. This value is higher than that previously reported in [20]. This is because it is compared in 3-D, and the air gap has been calculated more accurately (the thickness of the gauss meter probe has also been considered). When the inner

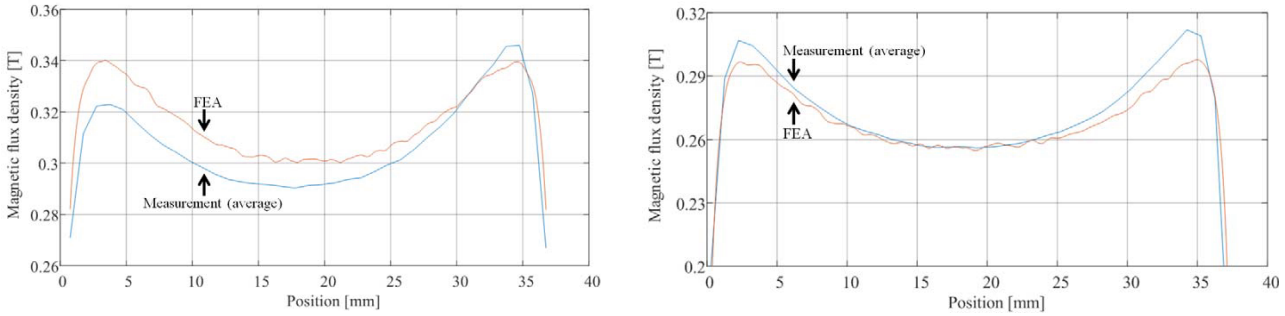

Figure 17. (a) Inner magnets field comparison with a 3-D FEA magnetostatic model and (b) outer magnet field comparison along the central axial length of the magnet with an air gap of 0.57 mm when $B_r = 1.03$ T.

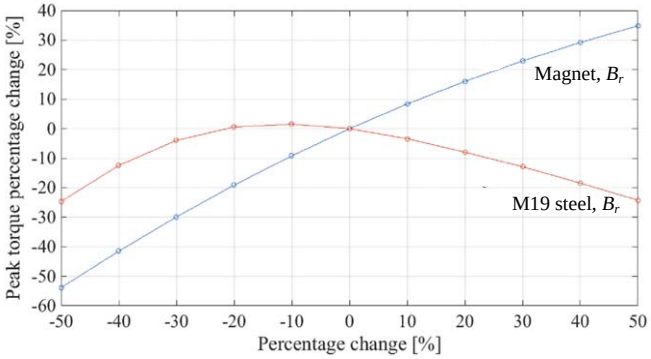

Figure 18. The relationship between the percentage change in peak torque with the percentage change in the B_r of the M19 steel and NdFeB magnet material.

and outer magnet residual flux density, B_r, values were reduced to match the average value measured in Figure 16, the calculated peak static torque using 3-D FEA was determined to be $T_2 = 77$ Nm which is 7% higher than the measured peak static torque of 71.7 Nm.

The authors believe that the magnets reduced residual flux density, B_r, was caused by the magnets being demagnetized during earlier testing. The initial laminated MG design, not shown here, had an inferior endplate retaining structure that resulted in the end plates not properly centering the rotors. This resulted in an eccentricity and it is believed that significant heating occurred that partially demagnetized the magnets. The authors then modified the design (to that shown in Figure 10) to ensure that the design was more robust.

If the mechanical structure is designed as expected, there are two primary magnetic material factors that will affect the peak torque of the MG. They are the magnet and steel residual magnetic flux density, B_r. A sensitivity analysis was conducted to ascertain how these two magnetic properties affected the torque. The results are shown in Figure 18. The percentage change in the torque when the magnets' B_r changes clearly dominates and is relatively linear.

6. EFFICIENCY ANALYSIS

The power relation between rotors is

$$T_2\omega_2 + T_1\omega_1 = P_l \tag{5}$$

where the power loss, P_l, is defined as

$$P_l = P_f + P_e \tag{6}$$

where P_f = friction and windage loss and P_e = eddy current and hysteresis loss. Note the torque, T_1, on the inner rotor in Eq. (5) is negative as the torque on the cage rotor opposes the torque created on

both the outer and inner rotor. The efficiency of an MG can be computed from

$$\eta = \frac{|T_1|\omega_1}{|T_2|\omega_2} \tag{7}$$

since the speed ratio given by Eq. (3) must be maintained when the MG is not pole-slipping, the substitution of Eq. (3) into Eq. (7) enables the efficiency to be determined from

$$\eta = \frac{|T_1|}{|T_2|} G_{12} \tag{8}$$

Using Eq. (8) the efficiency at different load conditions was measured as shown in Figure 19. The electrical losses are not a function of load, and therefore the efficiency increases with increasing load. Table 3 shows the calculated loss values as well as torque at $\omega_2 = 300$ RPM when using the 2-D FEA and 3-D FEA models with and without including the end-plates. The eddy current loss is primarily within the cage rotor rods and outer rotor magnets. These parts see the highest frequencies. The end-plates have a marked effect on increasing the loss. The difference in the measured and calculated losses is believed to be associated with the mechanical frictional losses. Table 3 also shows that the 3-D axial edge effects along with end plate eddy current losses reduce the peak torque by 13%.

Several authors locate the cage rod supports within the ferromagnetic slot air region [2, 11, 12]. To determine the impact of this on the efficiency an analysis was conducted for the two cases shown in Figure 20. In Figure 20(a) ferromagnetic cage rods are used within the cage bars, whilst in Figure 20(b) non-magnetic steel rods are used between the cage segments. Table 4 summarizes the results. Interestingly, it can be noted when the rods are within the ferromagnetic segment the loss is lower.

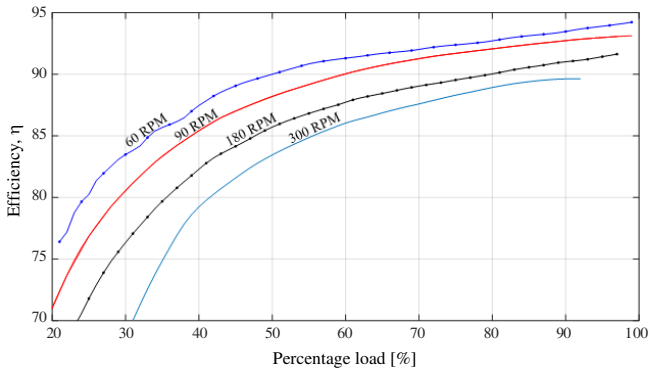

Figure 19. Measured efficiency as a function of percentage load for different ω_1 values on the low speed cage rotor. The 100% full load occurred at the peak torque condition ($T_2 = 71.7\,\text{Nm}$).

Table 3. Summary of the efficiency analysis when $\omega_2 = 300$ RPM.

Description	Magnets [W]		Rods [W]		End plates [W]	Total Loss [W]	Efficiency [%]	Peak Torque [Nm]
	Inner rotor	Outer rotor	Cage Rotor	Inner and outer rotor				
2-D	1.7	24.2	32.4	0.4	0	58.7	97.9	87.5
3-D — no end-plates	0.4	2.3	2.7	0.05	0	5.45	99.8	77.9
3-D — with end-plates	1.3	36.2	29.1	0.9	46.0	113.5	95.3	77.1
Measured (at peak load)	-	-	-	-	-	218	89.6	66.5

(a) (b)

Figure 20. Modified design when (a) mechanical support 416 stainless steel cage rods are at the center of the ferromagnetic slots and (b) mechanical support 316 non-magnetic cage rod are inserted into Garolite support inserts.

Table 4. Cage segment loss analysis when $\omega_2 = 300$ RPM.

Cage rod design approach	Magnets [W]		Rods [W]		End plates [W]	Total Loss [W]	Efficiency [%]
	Inner rotor	Outer rotor	Cage Rotor	Inner and outer rotor			
(a) Within cage segment	3.7	44.2	42.0	1.1	0	91.0	97.5
(b) Between cage segment	3.6	42.7	72.9	2.6	0	121.8	96.7

7. CONCLUSIONS

A flux focusing MG typology analysis was conducted, and a new fully laminated flux focusing MG structure was presented that is relatively easy to assemble. The design is unique in that the low speed cage rotor does not need to rely on epoxy or other complex fabrication steps to construct it. The experimentally measured peak torque density was 71.7 Nm (97 Nm/L) which was 30% lower than the 2-D calculated value. It was determined that the torque was lower than expected due to the magnets being demagnetized. A 3-D eddy current loss analysis was also conducted that highlighted the need for using non-conductive end plates.

ACKNOWLEDGMENT

The authors would gratefully like to thank the JMAG Corporations for the use of their FEA software. This material is based upon work partially supported by the Department of Energy under Grant No. DE-EE0006801 as well as the University of North Carolina Coastal Studies Institute NC Renewable Ocean Energy Program Grant.

REFERENCES

1. Martin, T. B., "Magnetic transmission," USA Patent 3,378,710, 1968.
2. Atallah, K., S. D. Calverley, et al., "Design, analysis and realisation of a high-performance magnetic gear," *IEE Proc.-Electr. Power Appl.*, Vol. 151, 135–143, 2004.
3. Rasmussen, P. O., T. O. Andersen, et al., "Development of a high-performance magnetic gear," *IEEE Trans. Ind. Appl.*, Vol. 41, 764–770, 2005.
4. Li, X., K.-T. Chau, M. Cheng, and W. Hua, "Comparison of magnetic-geared permanent-magnet machines," *Progress In Electromagnetics Research*, Vol. 133, 177–198, 2013.
5. Jian, L. and K.-T. Chau, "Analytical calculation of magnetic field distribution in coaxial magnetic gears," *Progress In Electromagnetics Research*, Vol. 92, 1–16, 2009.
6. Lipo, T. A., *Introduction to AC Machine Design*, 2nd Edition, Madison, 2004.
7. Uppalapati, K. K., W. Bomela, et al., "Experimental evaluation of low speed flux focusing magnetic gearboxes," *IEEE Trans. on Ind. Appl.*, Vol. 50, 3637–3643, Nov./Dec. 2014.
8. Uppalapati, K. K., J. Z. Bird, et al., "A magnetic gearbox with an active region torque density of 239 Nm/L," *IEEE Trans. Ind. Appl.*, Vol. 54, 1331–1338, Apr. 2018.
9. Uppalapati, K. K. and J. Z. Bird, "An iterative magnetomechanical deflection model for a magnetic gear," *IEEE Trans. Mag.*, Vol. 50, No. 2, 7005904, 2014.
10. Jian, L., G. Xu, J. Song, H. Xue, D. Zhao, and J. Liang, "Optimum design for improving modulating-effect of coaxial magnetic gear using response surface methodology and genetic algorithm," *Progress In Electromagnetics Research*, Vol. 116, 297–312, 2011.
11. Rasmussen, P. O., T. V. Frandsen, et al., "Experimental evaluation of a motor-integrated permanent-magnet gear," *IEEE Trans. Ind. Appl.*, Vol. 49, 850–859, 2013.
12. Gerber, S. and R. J. Wang, "Design and evaluation of a magnetically geared PM machine," *IEEE Trans. Magn.*, Vol. 51, 1–10, 2015.
13. Frandsen, T. V., P. O. Rasmussen, et al., "Improved motor intergrated permanent magnet gear for traction applications," *IEEE 2012 Energy Conv. Cong. Expo.*, 3332–3339, Raleigh, NC, 2012.
14. Frank, N. W. and H. A. Toliyat, "Analysis of the concentric planetary magnetic gear with strengthened stator and interior permanent magnet inner rotor," *IEEE Trans. Ind. Appl.*, Vol. 47, 1652–1660, Jul. 2011.
15. Gouda, E., "Transmission planetaire magnetique etude, optimisation et realisation," Ph.D. Disertation, Nancy Universit, France, 2011.
16. Kowol, M., J. Kolodziej, et al., "Impact of modulator designs and materials on efficiency and losses in radial passive magnetic gear," *IEEE Trans. Energy Conv.*, 1–1, 2018.
17. Kim, S.-J., E.-J. Park, et al., "Optimal design of ferromagnetic pole pieces for transmission torque ripple reduction in a magnetic-geared machine," *Journal of Electrical Engineering & Technology*, Vol. 11, 1628–1633, Nov. 2016.
18. Liu, J., W. Zhao, et al., "A novel flux focusing magnetically geared machine with reduced eddy current loss," *Energies*, Vol. 9, 904–919, Nov. 2016.
19. Jian, L., K. T. Chau, et al., "A magnetic-geared outer-rotor permanent-magnet brushless machine for wind power generation," *IEEE Trans. on Ind. Appl.*, Vol. 45, 954–962, 2009.
20. Uppalapati, K., K. J., et al., "A low assembly cost coaxial magnetic gearbox," *South. Power Elec. Conf.*, Auckland, NZ, Dec. 5–8, 2016.
21. Nobuhara, S., H. K. Niguchi, et al., "Proposal of new-shaped pole pieces for a magnetic-geared generator," *International Journal of Applied Electromagnetics and Mechanics*, Vol. 52, 763–769, 2016.